Assessing representativity of NH₃ measurements influenced by boundary-layer dynamics and turbulent dispersion of a nearby emission source

Ruben B. Schulte[1], Margreet C. van Zanten[1,2], and Jordi Vilà-Guerau de Arellano[1]

[1]Wageninen University & Research, P.O. Box 47, 6700, AA Wageningen, the Netherlands
[2]National Institute for Public Health and the Environment (RIVM), Antonie van Leeuwenhoeklaan 9, 3721, MA Bilthoven, the Netherlands

Correspondence: Ruben Schulte (ruben.schulte@wur.nl)

Abstract.

This study presents a fine scale simulation approach to assess the representativity of ammonia (NH₃) measurements in proximity of an emission source. Close proximity to emission sources (< 5 km) can introduce a bias in regionally representative measurements of the NH₃ molar fraction and flux. Measurement sites should therefore be located a significant distance from

5 emission sources, but such requirements are poorly defined and can be difficult to meet in densely agricultural regions. This study presents a consistent criterium to assess the regional representativity of NH₃ measurements in proximity of an emission source, calculating variables that quantify the NH₃ plume dispersion using a series of numerical experiments at a fine resolution (20 m). Our fine scale simulation framework with explicitly resolved turbulence enables us to distinguish between the background NH₃ and the emission plume, including realistic representations of NH₃ deposition and chemical gas-aerosol trans-

10 formations. We introduce the concept of blending-distance, based on the calculation of turbulent fluctuations, to systematically analyze the impact of the emission plume on simulated measurements, relative to this background NH₃. This sensitivity analysis includes systematic experiments varying meteorological factors, emission/deposition and NH₃ dependences. Considering these sensitivities, we find that NH₃ measurements should be located at a minimum distance of 0.5 - 2.5 km and 1 - 3.5 km from an emission source, for NH₃ molar fraction and flux measurements respectively. The simulation framework presented here can

15 easily be adapted to local conditions and paves the way for future ammonia research at high spatio-temporal resolution.

1 Introduction

Excess atmospheric nitrogen leads to an increased public health risk, through the formation of particulate matter, and causes environmental damage, as nitrogen deposition leads to eutrophication, ecosystem acidification and shifts in climate change (Erisman and Schaap, 2004; Sutton et al., 2008; Behera et al., 2013; Erisman et al., 2013; Smit and Heederik, 2017). There can

20 be serious societal consequences when nitrogen deposition critical loads are exceeded, as is the case in the Netherlands where the nitrogen crisis threatens the Dutch environment and economy (Stokstad, 2019). Atmospheric ammonia (NH₃) plays a key

role in this process, mainly originating from agricultural activities and accounting for two-thirds of all nitrogen deposition in the Netherlands between 2005 and 2016 (Wichink Kruit and van Pul, 2018).

It is therefore important to have a network of NH_3 concentration and deposition measurements, used for model validation
25 and (trend) monitoring (Wichink Kruit et al., 2021). For these purposes, the measurement sites in such a network must be representative for a larger region. One requirement for such regional measurement sites is to be located at sufficient distance from local NH_3 sources, as local emissions introduce a bias in the observations (EMEP/CCC, 2001; Wichink Kruit et al., 2021). Positioning measurements sites at sufficient distance from local sources is a challenge in densely agricultural areas like the Netherlands and regions all across the world with intensive livestock farming, e.g. North-West Germany, the province of
30 Lerida in Spain, the state of North-Carolina in the USA or the Hai River Basin in China.

The emitted NH_3 is transported and mixed within the convective boundary layer (CBL) through turbulent dispersion. The field of turbulent plume dispersion is extensively researched using both observations and turbulent resolved models. However, such studies typically focus on concentration peaks of highly toxic/flamable gasses (Mylne and Mason, 1991; Ardeshiri et al., 2021; Cassiani et al., 2020), quantification of the emission strength and position (Shah et al., 2020; Ražnjević et al., 2021) or
35 on statistical descriptions of the emission plume (Barad, 1958; Dosio et al., 2003; Vrieling and Nieuwstadt, 2003; Dosio and Vilà-Guerau de Arellano, 2006), typically used in chemistry transport models, e.g. OPS (Sauter et al., 2018), LOTOS-EUROS (Schaap et al., 2008) or EMEP MSC-W (Simpson et al., 2012). These transport models typically operate with resolutions at kilometer scale (1 - 50 km) and parameterized turbulence, making them unsuitable to study the impact of local NH_3 sources on nearby measurement sites at the subkilometer scale.

40 Furthermore, plume dispersion studies generally focus on chemically inert gasses, e.g. methane (Shah et al., 2020; Ražnjević et al., 2021). Ammonia is highly reactive: surface-atmosphere exchange and chemical gas-aerosols transformations play an important role in the NH_3 budget (Fowler et al., 1998; Van Oss et al., 1998; Nemitz et al., 2004; aan de Brugh et al., 2013; Behera et al., 2013; Shen et al., 2016; Schulte et al., 2021). Additionally, ammonia emissions in densely agricultuural areas are released and mixed into a background concentration, a result of long range transport of NH_3 (10-100 km). Yearly averaged
45 background concentrations can vary from 1-2 μg m^{-3} (e.g in coastal regions) up to up to tens of μg m^{-3} in regions with intensive agricultural activity, which is the focus on this study (van Zanten et al., 2017).

In this study, we investigate the impact of a typical ammonia emission source on the regional representativeness of NH_3 concentration and flux measurements. The novelty of our approach is twofold:

– The use of a fine scale Large-Eddy Simulation (LES) model with explicitly resolved turbulence at a very high spatio-
50   temporal resolution (10-100 m and 10 s - 1 min).

– Inclusion of realistic representations of surface-atmosphere exchange, chemical gas-aerosol transformations and a back-
   ground ammonia concentration.

Following this approach, we combine fine scale simulations, where turbulence is explicitly resolved, with concepts of theory on turbulent emission plume dispersion and translate this knowledge to practical applications for the measurement community.
55 The aim is to carry out a systematic analysis on how meteorological factors, including boundary-layer dynamics, deposition,

chemical transformation and model resolution influence the relationships between emission and receptor. To this end, we indroduce and analyze the concept of a blending-distance (BD), i.e. the horizontal distance at which the emission plume can be considered well-mixed with respect to the background NH_3. With the concept of blending-distance, we aim to provide an estimate of the minimum required distance from a typical NH_3 emission source for regionally representative measurements.

2 Methodology

2.1 NH_3 turbulent dispersion in DALES

To understand the variations of the NH_3 budget due to turbulence and heterogeneous sources and sinks of ammonia, our approach is two folded: (a) explicit simulation of processes that govern turbulent dispersion and mixing of NH_3 and (b) identifying their individual contributions to the NH_3 molar fraction and surface-atmosphere exchange. For the former, we use the large-eddy simulation technique with a high resolution to solve explicitly turbulence. To this end, we conduct our numerical experiments using a modified version of the Dutch Atmospheric Large-Eddy Simulation (DALES) version 4.2 (Heus et al., 2010; Ouwersloot et al., 2017), with the original v4.2 freely available online (at http://doi.org/10.5281/zenodo.3759193). DALES explicitly resolves processes at scales ranging from hundred meters to kilometres, using filtered Navier-Stokes equations with the Boussinesq approximation. The filter size is generally equal to the grid size of the simulations, with subfilter-scale processes being parameterized using one-and-a-half-order closure. The numerical experiments presented here are performed using a 20 m x 20 m x 5 m grid for a 10 km x 4.8 km x 3 km domain (500 x 240 x 600 grid points). Atmospheric NH_3 is added to DALES as a passive scalar in ppb, of which the spatial evolution is solved simultaneously with the thermodynamic variables. The boundary conditions for scalars and meteorological variables are periodic, unless stated otherwise.

The atmospheric ammonia budget is further governed by surface-atmosphere exchange and chemical gas-particle transformations (Schulte et al., 2021). We use a simplified, yet realistic, approach in our representation of these processes. NH_3 surface-atmosphere exchange is modelled by a constant homogeneous deposition of 0.045 ppb m s^{-1} (about 0.032 μg m^{-2}s^{-1}), representative for the observed yearly average NH_3 dry deposition in the Netherlands (https://www.rivm.nl/stikstof/meten/drogedepositieNH3; Stolk et al., 2014). The representation of the chemical gas-aerosol transformations follows the approach of the OPS model: applying a percentage per hour change in the molar fraction of gaseous NH_3 to the whole domain (van Jaarsveld, 2004).

Special attention is placed on the representation of the one NH_3 emission source in our domain, representing a dairy barn. Agricultural activity accounts for over 90% of the NH_3 emissions in the Netherlands and the European Union (Anys et al., 2020; Vonk et al., 2020; van Bruggen et al., 2021). Dairy farms account for approximately 50% of these agricultural NH_3 emissions, with approximately 15.000 farms with about 100 cows each on average in the Netherlands (van der Peet et al., 2018; WUR, 2021). A typical cubicle stable for 80 cows has a yearly emission of about 800 kg NH_3 year^{-1} and requires 10 m^2 per cow (800 m^2 in total) (Remmelink et al., 2020, Table 10.19; RIVM, 2021, type A1). Contrary to the closed off and air filtered housing for pigs and chickens, a dairy barn is open and the ammonia-rich air can freely escape. Therefore, we are able

to represent a typical 80 dairy cow barn as a surface emission source (Theobald et al., 2012) with an emission flux of 45 ppb m s^{-1} (about 32 μg m^{-2}s^{-1}) over an area of 800 m^2.

90   We identify the individual contributions of ammonia sources to the NH$_3$ molar fraction and surface-atmosphere exchange, with each source of NH$_3$ represented by a unique scalar. In this study, these sources are identified as a background molar fraction (NH$_{3,bg}$) and the NH$_3$ emission plume (NH$_{3,plume}$) from a surface emission source. The sum of these two unique scalars represents the total atmospheric ammonia (NH$_{3,total}$), as would be observed by in-field observations. Here, we modify DALES v4.2 to force the NH$_{3,plume}$ molar fraction to zero at both x-edges of the domain (west and east), preventing circulation

95   of the emission plume in x-direction.

Further modifications to DALES v4.2 are made to include the remaining processes governing the variability of the atmospheric ammonia budget. The scalar surface flux (F$_{total}$), representing surface atmosphere exchange, is divided between a flux acting on the background scalar (F$_{bg}$) and another flux acting on the emission plume scalar (F$_{plume}$). The magnitude of these two fluxes is weighted by their respective molar fractions (NH$_{3,bg}$ and NH$_{3,plume}$) relative to the total NH$_3$ molar fraction, e.g.

100   $F_{bg} = \frac{NH_{3,bg}}{NH_{3,total}} F_{total}$ for NH$_{3,bg}$.

The final modification adds an additional term to be added to the change in the scalar molar fraction ($\frac{S}{dt}$). This modified change in the scalar molar fraction reads: $\frac{dS}{dt} + \frac{R_{chem}}{3600} S$, with R$_{chem}$ representing the gain/loss rate in % hour^{-1} and subscript S representing the scalar molar fraction, which can be substituted by either NH$_{3,plume}$ or NH$_{3,bg}$.

2.2   Numerical experiments

105   We simulate the meteorological conditions observed on 8 May 2008 at the CESAR – Ruisdael Observatory (https://ruisdael-observatory. nl/cesar/) in the Netherlands (51.971ºN, 4.927ºE), as described by aan de Brugh et al. (2013) and Barbaro et al. (2014, 2015). This case is selected as it is widely studied and includes measurements of the NH$_3$ molar fraction. In May 2008, the intensive observational campaign IMPACT/EUCAARI was held, which included ammonia concentration measurements by a MARGA system (aan de Brugh et al., 2012; Mensah et al., 2012) and several additional meteorological variables, including vertical

110   profiles and radiosondes (Kulmala et al., 2011). The model is initialized following the conditions as described by Barbaro et al. (2014). The case can be characterized as typical clear-sky, fair-weather conditions with an absence of large-scale heat advection. The initial and prescribed meteorological values of the reference experiment can be found in Barbaro et al. (2014) Table 1, where the experiment is called CESAR2008.

In the morning, a 1500 m residual layer leads to a very rapid growth of the CBL around 10:30 CEST, up to roughly 1800

115   m. In the afternoon (12:30 – 17:00 CEST), CBL growth is weak and the thermodynamic conditions remain relatively constant (Barbaro et al., 2014). Therefore, we only study the turbulent dispersion in the afternoon, when the impact of boundary layer dynamics on the NH3 budget is minimal. The wind speed is moderate at 5.5 to 7 m s^{-1} in the afternoon, resulting in strong shear production near the surface and a strong momentum entrainment at the CBL top. The convective time scale (τ) in the

afternoon is typical for convective fair-weather conditions, increasing from 18 to 27 minutes between 12:30 and 17:00 CEST.
120   The Monin-Obukhov length fluctuates around approximately -50 m.

The numerical experiments are split into three phases: the meteorological spin-up phase, the buffer phase and the analysis phase. During the meteorological spin-up, 8:00 – 12:30 CEST, the ammonia surface-atmosphere exchange and chemical transformations are not active. These processes are activated at the start of the buffer phase, from 12:30 – 14:00 CEST. Entrainment is still an important factor until around 13:00 CEST, causing large fluctuations of the NH_3 molar fraction (> 4 ppb) as will
125   be discussed in Sect. 3.1. The CBL is considered well-mixed around 13:00 CEST, but we extend the buffer phase with one more hour. We do so to minimize impact of earlier entrainment on the one-hour moving average used to calculate statistics during the analysis phase. The analysis phase therefore starts at 14:00 CEST until the collapse of the CBL around 17:00 CEST. The analysis phase is the focus of this study and when we analyze the impact of the emission plume on (simulated) point measurements of the NH_3 concentration and flux.

130   **2.3   Quantifying the emission plume impact on NH_3 measurements**

Inspired by the plume observation study by Mylne and Mason (1991), we introduce three variables to assess the presence of the emitted NH_3 plume and relevance of the plume fluctuations to nearby observations. These variables, intermittency factor (I), fluctuation intensity (fI) and NH_3 flux (F), are all defined by fluctuations in the NH_3 molar fraction. Fluctuations in the NH_3 molar fraction result from turbulent mixing of differences in NH_3, caused by local sinks and sources. NH_3 fluctuations
135   are therefore found in the background molar fraction as a result of ammonia-poor air near the surface (deposition) and top of the CBL (entrainment). NH_3 fluctuations are further enhanced in proximity of surface heterogeneous surfaces. A strong local emission source (e.g. a dairy barn) as presented in this study, will cause an emission plume as the enhanced NH_3 molar fraction is mixed with the background molar fraction through turbulent mixing. Turbulent models like DALES explicitly resolve this turbulent mixing at high spatial-temporal resolution and can provide valuable information in the interpretation of in-field
140   observations where surface heterogeneity plays an important role.

We first introduce the intermittency factor (I) to quantify the detectability of the emission plume. Intermittency is defined as the proportion of time during which the plume molar fraction is above the detection limit of instruments typically used to measure atmospheric ammonia, as seen in Fig. 1 and Eq. 1, where N is the number of timesteps.

$$I = \frac{1}{N} \sum_{i=1}^{N} \begin{cases} 1, & \text{if } NH_{3,plume}(i) \geq 0.25ppb \\ 0, & \text{if } NH_{3,plume}(i) < 0.25ppb \end{cases} \tag{1}$$

145   Note that the intermittency is calculated for each individual grid point during the analysis window (14:00 - 17:00 CEST) at 10 s temporal resolution. We set the NH_3 detection limit at 0.25 ppb, similar to the detection limit of the miniDOAS instrument used in the Dutch ammonia monitoring network (Berkhout et al., 2017). The concept of intermittency cannot be applied to $NH_{3,bg}$ or $NH_{3,total}$, as the background molar fraction always exceeds 0.25 ppb in our numerical experiments, which would result in an intermittency of 1. We therefore only calculate the intermittenct for $NH_{3,plume}$ to analyze the detectability of the
150   emission plume.

Figure 1. Top panel shows 10 s time series of $NH_{3,total}$ (orange) and $NH_{3,plume}$ (yellow) during the analysis phase, at 250 m from the emission source. The detrended $NH_{3,total}$ (orange) is shown in the bottom panel. Fluctuation intensity and intermittency are calculated following Eq. 4 and 1 respectively, based on the mean $NH_{3,total}$, standard deviation (light purple) and NH_3 detection limit (dotted black).

The second variable, fluctuation intensity (fI), determines the magnitude of the NH_3 fluctuations, i.e. NH_3 standard deviation (σ_{NH_3}), relative to the mean NH_3 molar fraction ($\overline{NH_3}$). Fluctuation intensity is defined following Eq. 2:

$$fI = \frac{\sigma_{NH_3}}{\overline{NH_3}} \tag{2}$$

The fluctuation intensity quantifies the level of turbulent mixing. High fI indicates that there are large fluctuations in the
155   measured NH_3 which can introduce a positive bias in measurements. In the field of plume dispersion, high fI is found close to the source where plume meandering dominates the mixing process (Dosio and Vilà-Guerau de Arellano, 2006), or at the edge of the emission plume as a result of lateral entrainment of air from outside the plume (Mylne and Mason, 1991; Gailis et al., 2007; Ražnjević et al., 2021). When analyzing the fluctuation intensity of $NH_{3,total}$, we have a consistent reference for the fluctuation intensity in $NH_{3,bg}$. Comparing the fI for the total ammonia (fI$_{total}$) to the fI for the background ammonia (fI$_{bg}$),
160   enables us to quantify the relative impact of the emitted NH_3 plume to simulated measurement. When fI$_{total}$ is of the same order of magnitude as fI$_{bg}$, we consider the emission plume indistinguishable from the background NH_3, i.e. the plume is well mixed.

Note that Fig. 1 shows a downward trend in $NH_{3,bg}$ and $NH_{3,total}$, resulting from surface deposition and the loss by chemical gas-aerosol transformations. To minimize the impact of this downward trend on σ_{NH_3}, we detrend the simulated molar fraction
165   by subtracting a 1 hour leading moving average ($NH_{3,MA}$), following Eq. 3 and shown in Fig. 1. The detrended molar fraction ($NH_{3,detrend}$) is assumed to only represent turbulent fluctuations and is used to calculate the standard deviation to derive fluctuation intensity. By using $NH_{3,detrend}$ to calculate σ_{NH_3}, the fluctuation intensity follows from Eq. 4.

$$NH_{3,detrend} = NH_3 - NH_{3,MA} \tag{3}$$

$$fI = \frac{\sigma_{NH_3}}{\overline{NH_3}}$$
$$= \frac{\sqrt{\frac{1}{N-1}\sum_{i=1}^{N}|NH_{3,detrend} - (\overline{NH_{3,detrend}})|^2}}{\overline{NH_3}} \tag{4}$$

Finally, we introduce the 30 minute NH_3 flux, studied to mimic the in-field ammonia eddy-covariance flux measurements and calculated following Eq. 5. The flux presented in this study is the average 30 minute flux, for each individual grid point, over the analysis phase between 14:00 and 17:00 CEST.

$$F_{NH_3} = \overline{NH_3'w'} \tag{5}$$

2.4 The concept of blending-distance

We use the fluctuation intensity and flux to quantify the impact of the emission plume on the simulated NH_3 molar fraction and flux measurements, by introducing the concept of blending-distance. The blending-distance is based on the percentage change (PC_X) in the simulated NH_3 measurements resulting from the emission plume, i.e. the percentage change between $NH_{3,total}$ and $NH_{3,bg}$. PC_X is calculated following Eq. 6, where X can be substituted by either fI or F.

$$PC_X = |\frac{X_{total} - X_{bg}}{X_{bg}}| * 100\% \tag{6}$$

Based on this percentage change, we define a threshold for which we assume that the impact of the emission plume is negligible. The blending-distance (BD_X, is defined as the maximum distance at which PC_X drops below the threshold level (e.g. $PC_X < 10\%$), following Eq. 7.

$$BD_X = max(\ dist(\ PC_X < threshold\ )\ ) \tag{7}$$

In this study, we present blending-distances based on an arbitrary set of threshold levels, ranging from 5% to 50%.

The concept of blending-distance is applied to the fluctuation intensity (BD_{fI}) and the NH_3 flux (BD_F) to quantify the impact on the simulated NH_3 measurements of NH_3 molar fraction and flux respectively. For context, we also present the intermittency in Sect. 3.2 to quantify the detectability of the plume.

2.5 Blending-distance sensitivity

A key aspect of the study is to determine the sensitivity of the concept of the blending-distance to variations in meteorological and NH_3 pollution factors. We study the sensitivity of blending-distance for fluctuation intensity and NH_3 flux by varying the

Table 1. Parameter names, symbols, reference values and their respective variations for the sensitivity study of the blending-distance, with the reference settings highlighted in bold.

Parameters	Symobol	Reference experiment	Variations				
Geostrophic wind speed	u_g	8 m s^{-1}		2 4 6 **8** 10			
Initial NH$_{3\,bg}$	C_{bg}	10		5 **10** 15 25			
NH$_3$ emission strength	E	45 ppb m s^{-1}		**45** 100 150 200			
NH$_3$ deposition strength	D	-0.045 ppb m s^{-1}	0 -0.025 **-0.045** -0.075 -0.0100				
NH$_3$ chemical conversion rate	R	5 % hour^{-1}		0 **5** 15 25			
Simulated measurement height	H	37.5 m	7.5 12.5 ... 112.5 117.5				
Model resolution	Δ	20 m x 20 m x 5 m	10 x 10 x 2.5 **20 x 20 x 5** 50 x 50 x 15				

geostrophic wind speed (u_g), initial background molar fraction (C_{bg}) at the start of the analysis phase, emission strength (E), deposition strength (D), chemical conversion rate (R), simulation height (H) and model grid resolution (Δ). Table 1 presents the suite of numerical experiments presented in this study. A single numerical experiment was performed for the sensitivity studies of the NH$_3$ background, emission, deposition and chemistry, each with separate scalars for NH$_{3,bg}$ and NH$_{3,plume}$, generating just under 1 TB of model output with a computational cost of about 64.000 SBU (System Billing Unit, i.e. the usage of one core of the Cartesius supercomputer system for one hour).

The sensitivity study is structured from large-scale processes to small scale processes and modelling numerics. Starting with mesoscale processes, we vary the geostrophic wind speed to study the impact of the atmospheric stability on blending-distrance, i.e. a shear or convection dominated CBL. Atmospheric stability plays a key role in turbulent mixing of local sources (emission) and sinks (entrainment and deposition), affecting both the fluctuations in the background molar fraction and the mixing of the emission plume (Dosio et al., 2003). Next, we study the sensitivity of BD to different levels of the background NH$_3$ at the start of the analysis window, representing different levels of regional NH$_3$ pollution. Additionally, varying the background levels of ammonia changes the NH$_3$ inversion at the top of the CBL, affecting the impact of entrainment. Next, the emission strength is varied, in order to study the local effect of different emission strengths.

Furthermore, we study the sensitivity of both BD$_{fl}$ and BD$_F$ to NH$_3$ deposition and the chemical gas-aerosol transformation. These are dynamic processes, i.e. experiencing clear diurnal and seasonal variability, mainly related to temperature, humidity and pollution levels (Wichink Kruit et al., 2010; van Zanten et al., 2010; aan de Brugh et al., 2013). Our simulation approach, with a simplified representation of deposition and chemistry, allows us to distinctly study the role of these two processes.

Finally, we study the sensitivity of BD to choices made in the numerical setup of the experiments. We vary the height of the simulated measurements. The numerical experiments are generally taken at a simulated height of 37.5 m. This is a trade-off between simulating measurements close to the surface to mimic in-field observations and the resolved turbulent kinetic energy (TKE$_{res}$) of the model. The TKE$_{res}$ at the lowest level of DALES (at 2.5 m) is zero due to the no-slip boundary at the surface
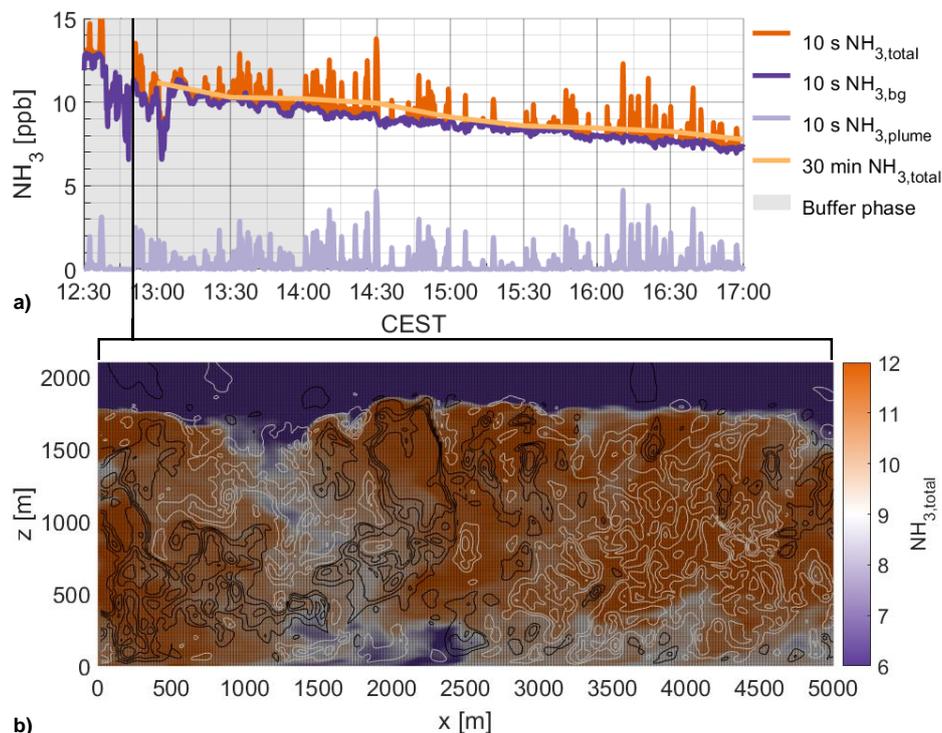
Figure 2. 10 s time series (a) of $NH_{3,total}$ (orange), $NH_{3,bg}$ (purple) and $NH_{3,plume}$ (light purple) during the buffer phase (grey area) and the analysis phase, taken at 250 m distance from the emission source. The large high-frequency fluctuations shown (> 4 ppb) are not captured by the 30 minute average of $NH_{3,total}$ (light orange). The vertical xz cross-section at 12:50 CEST (b), displays high spatial variability during the buffer phase in $NH_{3,total}$ (> 4 ppb) over short distances (hundreds of meters). The black/white contour lines represent upward/downward wind speed in steps of 0.5 m s^{-1}.

(Heus et al., 2010). When we aim for a TKE_{res} of 75% at all three (vertical) resolutions, we find TKE_{res} of 76%, 95% and 96% for the low, middle and high resolution at 37.5 m (36.25 m for high resolution). Additionally, it is also expected that varying
215 the measurement height will gain practical insight for in-field observations. Finally, the sensitivity of the blending-distance to changes in resolution is studied with two new numerical experiments with higher and lower resolutions of 10 m x 10 m x 2.5 m (1000 x 480 x 1200 grid points) and 50 m x 50 m x 15 m (200 x 96 x 200 grid points) respectively.

3 Results

3.1 Qualitative analysis of the NH₃ emission plume impact

220 The concept of blending-distance is based on fluctuations in the NH_3 molar fraction. To better understand the sources of these fluctuations, we first study the time series of a "virtual" point measurement at 250 m horizontal distance from the emission source, shown in Fig. 2a. Our simulation framework allows us to distinhuish the individual contributions to $NH_{3,total}$ (orange):

$NH_{3,bg}$ (purple) and $NH_{3,plume}$ (light purple). Here we find that the large $NH_{3,total}$ fluctuations are mainly ascribed to $NH_{3,plume}$. As discussed in Sect. 2.3, fluctuations are also found in the background concentration, $NH_{3,bg}$, leading to a non-zero fluctuation

225   intensity for the background molar fraction. The high-frequency fluctuations in $NH_{3,total}$ and $NH_{3,bg}$ are filtered out when averaging over 30 minutes, the typical averaging time of in-field observations. Such turbulent fluctuations could be interpreted as noise in the raw measurement data of in-field observations.

The NH_3 fluctuations in $NH_{3,bg}$ are a result of heterogeneous turbulent mixing of vertical molar fraction differences in the CBL. Both near the surface and the top of the CBL, the molar fraction decreases through surface-atmosphere exchange

230   (deposition) and turbulent exchange with the free troposphere (entrainment). A clear example of the impact of this turbulent mixing is shown in Fig. 2b, where the xz cross-section shows that entrainment causes a large pocket of ammonia-poor air (about 6 ppb) to reach the surface. This results in a sudden decrease of over 4 ppb in the simulated measurement, which can last for 5 to 15 minutes. The same process of turbulent mixing of local sinks and sources causes the fluctuations in the NH_3 molar fraction shown in Fig. 2a.

235   Now that we understand the source of the NH_3 fluctuations, we take a closer look at the emission plume without any background NH_3. We only calculate fI for $NH_{3,plume}$ for $\overline{NH}_{3,plume} > 1 \ 10^{-5}$. The xy plot in Fig. 3a shows low fI in the plume center (≈ 2) and a strong increase near the plume edges, up to fI ≈ 18. This is echoed by the plume transects, as they shows the typical "U-shape" found for Gaussian plumes (Mylne and Mason, 1991; Gailis et al., 2007; Ražnjević et al., 2021). These high fI values at the edges of the plume are a result of very low average molar fractions combined with low intermittency. This

240   leads to a high standard deviation, relative to the very low averaged molar fraction, at the plume edges. Without background NH_3, it is at the edges of the plume that in-plume lateral entrainment of ammonia-free air happens, diluting the emission plume by turbulent mixing.

The intermittency cross-section in Fig. 3b shows that maximum I is only a little over 0.3, resulting from the meandering of the plume. Figure 3b also shows that, with an NH_3 detection limit of 0.25 ppb, the plume can be detected up to a distance of

245   about 2.5 km from the source.

The cross-section of fI changes dramatically when analyzing $NH_{3,total}$, the sum of $NH_{3,bg}$ and $NH_{3,plume}$. With the addition of a non-zero background molar fraction, fI can be calculated over the whole domain, as shown in Fig. 3c. Now, we find a much lower fluctuation intensity, with a maximum of 0.08 for $NH_{3,total}$ compared to 18 for $NH_{3,plume}$. The U-shape in shown in the transect of Fig. 3a is replaced by an approximately Gaussian shape, with the highest fluctuation intensities at the centreline of

250   the plume. This centreline fI decreases with distance from the source and becomes indistinguishable from the out-of-plume fI after approximately 1 km distance, i.e. a rough estimate for BD_{fI}.

Finally, Fig. 3d shows that the emission plume leads to a positive flux (emission) for $NH_{3,total}$ in proximity of the emission source, while the flux is negative (deposition) outside the plume. Note that significant fluctuations are found in the flux over the full domain, with $\sigma_{F,bg} = 0.006$ ppb m s^{-1} (prescribed $F_{sfc.} = -0.045$ ppb m s^{-1}) for $NH_{3,bg}$. Similar to fI$_{total}$ in Fig. 3c, the

255   transects for the NH_3 flux are approximately gaussian in shape, with the peak values close to the plume centreline at y/y_{plume} = 0. After approximately 1 km at the approximate plume centreline, the in-plume flux becomes visually indistinguishable from
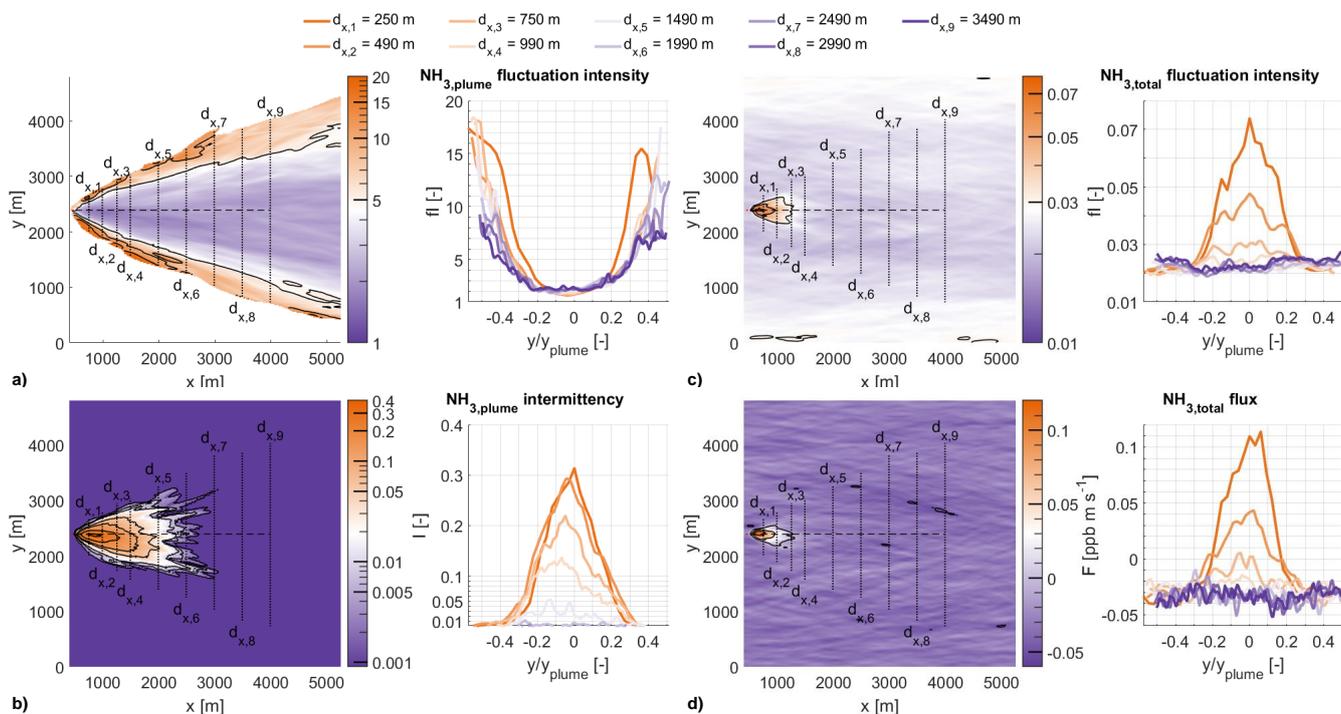
Figure 3. The xy cross-sections at 37.5 m with y-transects through the NH_3 emission plume for the $NH_{3,plume}$ fluctuation intensity (a), intermittency (b), $NH_{3,total}$ fluctuation intensity (c) and $NH_{3,total}$ flux (d). The plume transects are labelend $d_{x,1}$ to $d_{x,9}$ for increasing x-distance from the NH_3 emission source and normalized by plume width for $NH_{3,plume} > 1\ 10^{-5}$ ppb. The data presented is calculated during the analysis phase (14:00 and 17:00 CEST) at 37.5 m

.

the background, i.e. a rough estimate for BD_F. This positive anomaly is the result of the emission source being within the footprint of these receptors.

3.2 Quantitative analysis of the NH_3 emission plume impact

260   We apply the concept of blending-distance in Fig. 4 to the main variables that characterize the NH_3 evolution: fluctuation intensity (a), flux (b) and intermittency (c). The markers represent the value at each individual grid point on the 37.5 m horizontal plane, the continuous orange line represents the gridpoint with the highest value within a 50 m moving window (maximum statistics), the orange dotted line represents the plume centreline and the purple dashed and continuous lines represent the blending-distances for their respective threshold. Note that both the centreline and the maximum statistics give similar results, indicating that the highest values for fI, F and I are generally found at the plume centreline, though with uncertainties.

265   We interpret the calculation of the blending-distance based on 3 arbitraty threshold levels (5%, 25% and 50%) for fI and F, shown in Fig. 4a and b. The distance at which the maximum value of PC_X drops below the threshold level is the blending-
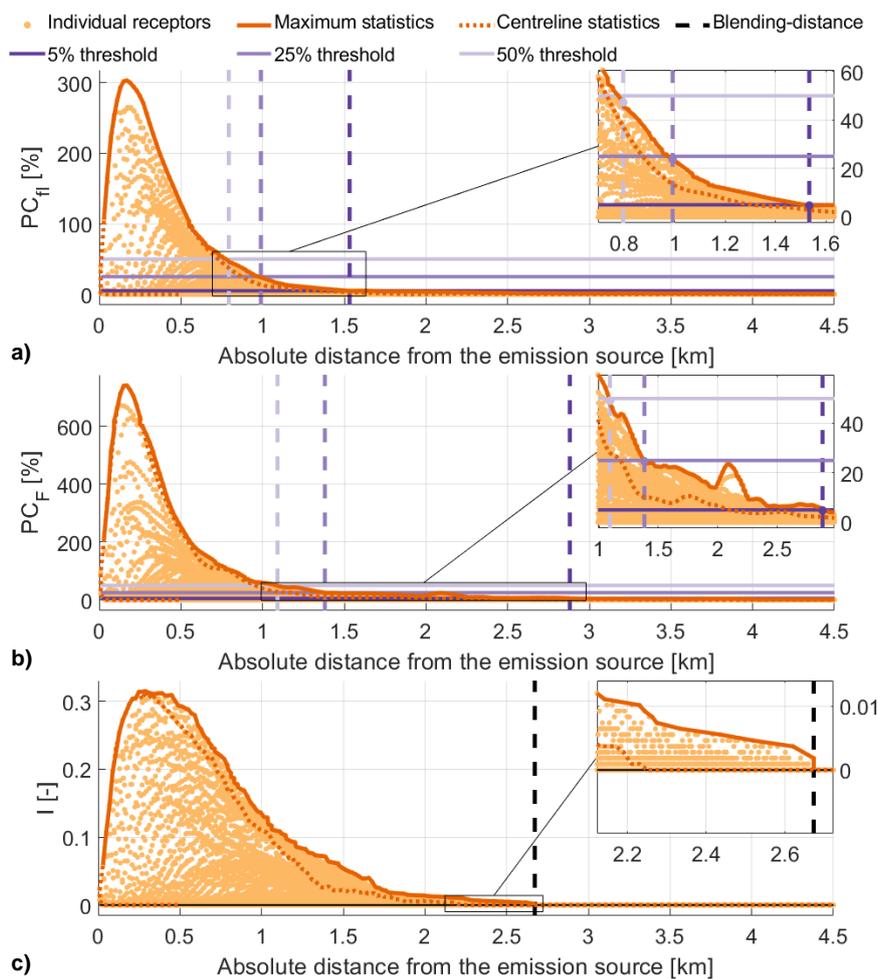
Figure 4. The percentage change of $NH_{3,total}$ relative to $NH_{3,bg}$ against absolute distance from the NH_3 emission source. The panels show fluctuation intensity (a), NH_3 flux (b) and intermittency (c). Highlighted are the maximum value within a 50 m moving window (orange) and the plume centreline (dotted orange). Blending-distances (purple dashed) are calculated based on three thresholds at 5%, 10% and 25% (purple continuous).

distance. The sensitivity of BD to these thresholds will be discussed in detail in Sect. 3.3, using Fig. 5 and 6. Additionally, we show the intermittency in Fig. 4c to show that the emission plume is quantifyable up to over 2.6 km distance.

270 Starting with the fluctuation intensity (Fig. 4a), PC_{fI} peaks at a relative change of about 300%, caused by the NH_3 emission plume. BD_{fI} decreases non-linearly from 1.5 km to 1 km with the thresholds increasing from 5% to 25%. We can therefore infer from BD_{fI} that, while the NH_3 plume is still quantifiable, the change in fluctuation intensity caused by the plume is < 5% at 1.5 km or less, depending on wind direction.

Figure 4b shows that the emission plume has a larger impact on NH_3 flux measurements than on measurements of the NH_3
275 molar fraction. The large difference between the emission strenght (45 ppb m s^{-1}) and the deposition (-0.045 ppb m s^{-1}) result in a maximum PC_F of nearly 750% in close proximity of the emission source and a long tail, indicating that the emission plume affects flux measurements over several kilometers. As a result, BD_F decreases from 2.9 km to 1.4 km for increasing thresholds, significantly longer distances then our 1 km qualitative estimate based on Fig. 3d. The fluctuations in F_{bg}, shown in Fig. 3d, translate to fluctuations in PC_F, as shown in the zoomed panel of Fig. 4b. Note that Fig. 3d shows that the flux changes sign in
280 proximity of the emission source and that this sign change is not reflected in Fig. 4b.

3.3 Sensitivity of blending-distance to meteorological and NH_3 pollution variables

We study the sensitivities of BD_{fI} and BD_F to a range of meteorological, NH_3 pollution parameters and model resolution and simulated measurement height (Table 1). The results of the sensitivity study are shown in Fig. 5 and 6 for an arbitrary set of threshold ranging from 5% (orange dashed) to 50% (orange dotted), representing the maximum acceptable difference in fI and
285 F caused by the emission plume in %.

Starting with BD_{fI}, Fig. 5 shows that BD_{fI} ranges roughly between 0.5 and 2.5 km; an indicating of the minimum distence for NH_3 molar fraction measurements. There is a negative correlation between BD_{fI} and the choice in threshold, i.e. increasing the threshold level decreases BD_{fI}. We generally find that BD_{fI} decreases nonlinearly by approximately 0.5 km when increasing the threshold level from 5% to 50%, halving BD_{fI}. We discuss the individual variables of Fig. 5 from top to bottom, starting
290 at the mesoscale (u_g), down to the micrometer scale (R) and finishing with the model resolution and simulated measurement heigh.

The geostrophic wind speed (u_g) is one of the main drivers of turbulent mixing and transport of the plume (Dosio et al., 2003; Vrieling and Nieuwstadt, 2003; Dosio and Vilà-Guerau de Arellano, 2006). Figure 5 shows that BD_{fI} is only weakly sensitive to u_g, showing a weak positive correlation between the two. By varying u_g we move from a convection-driven boundary
295 layer (u_g = 2 m s^{-1}) to more shear-driven meteorological conditions (u_g = 10 m s^{-1}). In a convection-driven boundary layer, turbulent mixing is rather weak and the NH_3 emission plume rises from the surface as convection plumes are the main drivers of turbulent mixing. Under these conditions, in-plume molar fractions are very high, but horizontal transport of the emission plume is weak, resulting in a low BD_{fI}. For shear-driven conditions, the NH_3 emission plume tends to stick to the surface as the increased horizontal wind speed enhances horizontal transport and turbulent mixing. The enhanced horizontal transport and
300 emission plume sticking to the surface should significantly increase BD_{fI}, but the enhanced turbulent mixing counteracts these processes by reducing the $NH_{3,plume}$ molar fraction and fluctuations. This is exactly what is shown in Fig. 5 and explains why
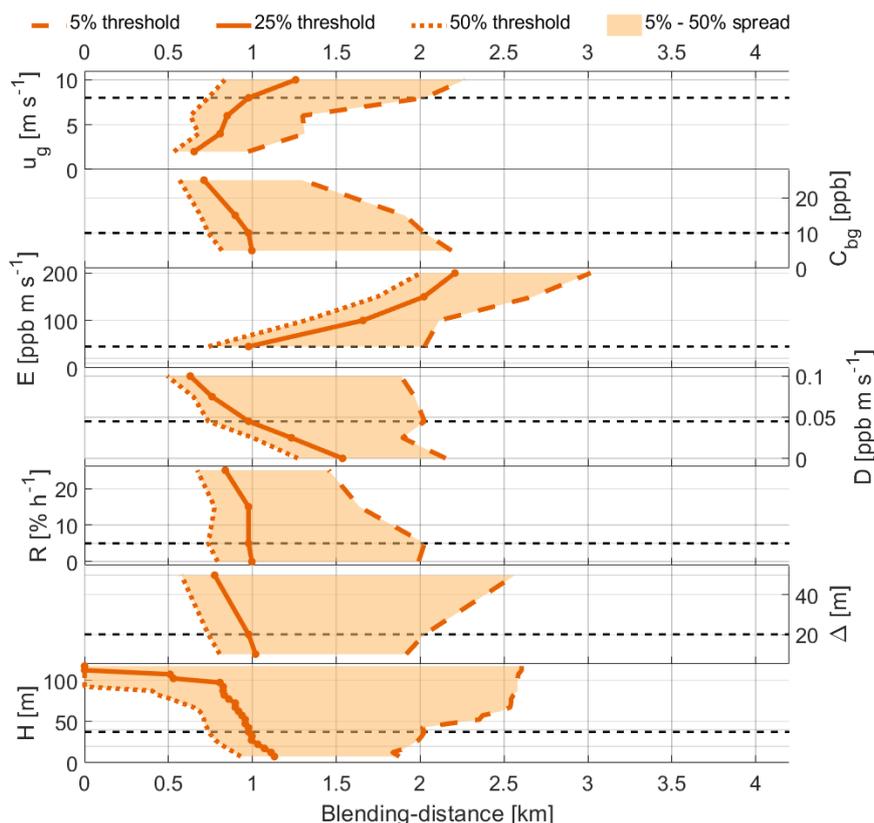
Figure 5. The sensitivity of BD_{fl} to the geostrophic wind speed (u_g), initial background molar fraction (C_{bg}), emission strength (E), deposition strenght (D), chemical reaction rate (R), model resolution (Δ) and simulated measurement height (H). BD_{fl} is determined for threshold levels ranging from 5% (orange dashed) to 50% (orange dotted).

the sensitivity of BD_{fl} increases for lower threshold levels (5%), as smaller plume fluctuations will reach long dinstances in shear-driven conditions.

One panel below, Fig. 5 shows a weak negative correlation between BD_{fl} and the initial background molar fraction (C_{bg}), i.e.
305 the regional level of NH_3 pollution. Increasing C_{bg} enhances the fluctuations in the CBL by entrainment, increaing σ_{bg} from 0.13 ppb (C_{bg} = 5 ppb) to 0.38 ppb (C_{bg} = 25 ppb). The relative weight of the $NH_{3,plume}$ fluctuations (σ_{plume}) decreases as a result, leading to slightly lower BD_{fl}.

At the local scale, Fig. 5 shows a clear positive and negative correlation when varying emission strength (E) and deposition strength (D) respectively. Both variables directly affect one of the main drivers of turblent mixing: heterogeneity. Increasing the
310 NH_3 emission strength of the local (heterogeneous) source directly increases fl_{plume}, increasing BD_{fl}. Varying the deposition on the other hand, directly affects the vertical NH_3 molar fraction gradient near the surface, increasing fl_{bg} for increasing D and reducing BD_{fl}. We only briefly touch upon the chemical conversion rate (R), as Fig. 5 shows that varying R does not significantly affect BD_{fl}. R is applied uniformly to the 3D domain and has little effect on turbulent mixing.
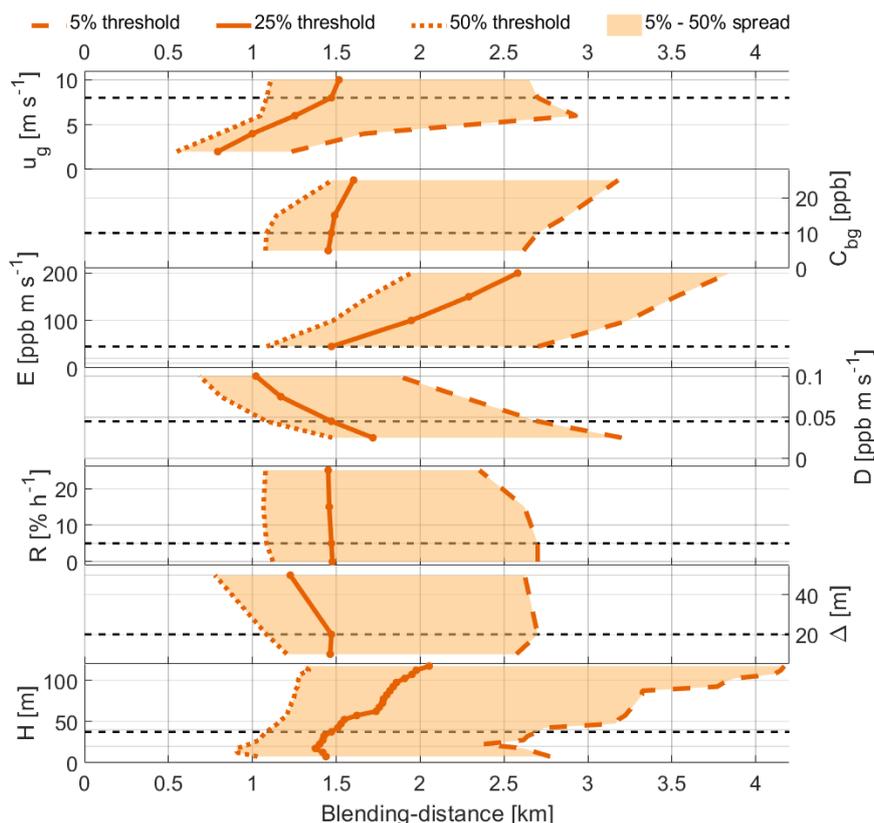
Figure 6. The sensitivity of BD_F to the geostrophic wind speed (u_g), initial background molar fraction (C_{bg}), emission strength (E), deposition strenght (D), chemical reaction rate (R), model resolution (Δ) and simulated measurement height (H). BD_F is determined for threshold levels ranging from 5% (orange dashed) to 50% (orange dotted).

Next, we vary the model resolution (Δ) in Fig. 5 and find that BD_{fl} is weakly sensitive to the model resolution. While the smallest fluctuations are not resolved by the model at $\Delta = 20 \times 20 \times 5$ m, the weak sensitivity of BD_{fl} indicates that this resolution is sufficient to infer the blending-distance.

Finally, Fig. 5 shows two regimes in the sensitivity of BD_{fl} to the simulated measurement height (H). For the 50% threshold, BD decreases by about 300 m with height up to 60 m. Above 60 m, there is a transition where BD_{fl} rapidly goes to zero. In this second regime, the simulated measurements are located above the plume centreline. From there on, fI_{plume} rapidly decreases with height until PC_{fl} does not reach the 50% threshold and BD_{fl} becomes zero. This rapid decrease is a result of the similated measurements being located above the emission plume, as the height of plume does not reach above 150 m for the first 1.5 km horizontal distance. The height of this transition increases with decreasing threshold levels as the thresholds become more sensitive to smaller $NH_{3,plume}$ fluctuations.

Figure 6 shows the results of the sensitivity study for BD_F (Table 1). Both the blending-distance for molar fraction measurements (BD_{fl}) and for flux measurements (BD_F) can be interpreted as a inverse footprint analysis, as we estimate the area

affected by the emission source. The results of the sensitivity study of BD_F however, could differ from the sensitivity study of BD_{fI}. The footprints for flux and molar fraction measurements are not the same and footprint for flux measurements are smaller than those of molar fraction measurements (Rannik et al., 2000; Kljun et al., 2003; Vesala et al., 2008). However, comparing BD_{fI} to the footprint of NH_3 molar fraction measurements is not straightforward, as BD_{fI} is based on the NH_3 fluctuation

330 intensity, not the molar fraction. It is therefore interesting to determine whether the results of the sensitivity study of BD_F will differ compared to the results of BD_{fI}.

When analyzing Fig. 6, we find that there are indeed differences between BD_F and BD_{fI}. BD_F is significantly longer, ranging from 1.0 to 3.5 km, indicating that NH_3 flux measurements are more sensitive to the emission plume. Note that we removed the results for D = 0 ppb m s^{-1}. Here, F_{bg} approaches zero, resulting in infinitely large PC_F and unrealistic BD_F values.

335 One of main differences between BD_F and BD_{fI} are found in the sensitivity to the threshold levels (5% to 50%). BD_F is more sensitive to the different threshold levels compared to BD_{fI}. This is in agreement with the results shown in Fig. 4b, where we discussed that PC_F is significantly larger than PC_{fI}, with a significanlty longer tail as well. Despite these differences, the same arbitrary set of thresholds are used for both BD_{fI} and BD_F. As a result, the non-linear effect of the aforementioned long tail in PC_F (Fig. 4b) increases BD_F for low threshold levels.

340 Significant differences between BD_F and BD_{fI} are also found in the sensitivity to the geostrophic wind speed (u_g) and the simulated measurement height (H). Both variables directly affect the footprint of the simulated flux measurements. In shear-driven turbulent conditions (high u_g), the footprint of the measurement is elongated compared to convective conditions. This reduces the width of the footprint and lengthens the up-wind distance at which the emission source can be measurement, thus increasing BD_F. Increasing H also increases the footprint of the measurements, but there is no elongation of the footprint. As

345 a result, BD_F has a strong positive correlation to u_g but is only weakly correlated to H.

There are also strong similarities between the sensitivity of BD_F and BD_{fI}. Both Fig. 5 and 6 show that the blending-distance is only weakly sensitive to the chemical reaction rate (R), initial background molar fraction (C_{bg}) and te model resolution (Δ). For both molar fraction and flux measurements, the emission strength (E), deposition (D) and the geostrophic wind speed (u_3 are the driving variables of the blending-distance.

350 ## 4   Discussion

4.1   Uncertainty on the blending-distance estimation

The blending-distance cannot be captured by a single number. The turbulent dispersion of the emission plume is chaotic by nature and driven by a wide range of factors. We therefore carry out a systematic analysis on how these factors, as well as the model resolution, influence the the relationships between emission and the simulated in-field measurements. Additionally, the

355 chaotic nature of turbulence introduces uncertainty in the blending-distances presented in this study, visualized and discussed in Sect. 3.1, where random spatial variability is seen in the fluctuation intensity and flux of $NH_{3,bg}$. This introduces an uncertainty in the blending-distance which is especially pronounced in the analysis of the NH_3 flux, as discussed in Sect. 3.2.

Furthermore, there is a downside to of our simplified representation of chemical transformations, in that it is applied uniformly to the 3D domain. In reality, the equilibrium molar fractions for these chemical transformations are related to temperature and humidity and results in a near-surface NH_3 gradient of the NH_3 molar fraction (aan de Brugh et al., 2013). Therefore, we are likely to underestimate the role of chemical transformations and overestimate BD_{fI}, as turbulent mixing of this near-surface gradient increases fI_{bg}.

Finally, we filter out the impact of boundary-layer dynamics and variations in the thermodynamic variables with our choice of analysis window, from 14:00 and 17:00 CEST. Bourndary-layer dynamics are especially relevant in the morning, when entrainment is one of the dominant processes driving the NH_3 diurnal variability (Wichink Kruit et al., 2007; Schulte et al., 2021). As shown in Fig. 2, entrainment leads to large fluctuations in $NH_{3,bg}$, increasing fI_{bg} and leading to a shorter BD_{fI}. Despite these uncertainties, the blending-distance provides a valuable first esitmate for the minimum distance required for measurements taken in proximity of a typical NH_3 emission source.

4.2 Blending-distance for passive tracers

Evaluating the blending-distance results against typical literature on plume dispersion is a complex exercise. These studies generally focus on the release of passive scalars in an unpolluted environment, with only few studies researching (near) surface releases (Cassiani et al., 2020). Normalization of both distance from the source as the plume molar fraction further complicates the interpretation of literature. We can make a rough estimate of blending-distance, using the modelled in-plume molar fraction by Dosio et al. (2003) and Dosio and Vilà-Guerau de Arellano (2006), which rapidly decreases for a convection-driven boundary layer ($-z/L \geq 40$ and $u_*/w_* \leq 0.2$) at the surface up to roughly 6 km distance, after which it levels off. This distance approximately doubles for shear-driven boundary layers ($-z/L \sim 40$ and $u_*/w_* \sim 0.46$). The observations by Mylne and Mason (1991) and the large-edy simulation results of Dosio et al. (2003) show that the in-plume fluctuation intensity also decreases with distance, but levels after roughly 15 km distance from the emission source.

These rough estimates of 6 to 15 km distance are significantly larger than the blending-distances presented in this study. Such long distances between source and measurement site would not make feasible requirements in densely agricultural regions, but are likely an overestimation of the blending-distance. These estimates are based on the molar fraction and fI of the emission plume, with no representation of background ammonia levels. The latter is especially important, as we show in Sect. 3.1 and 3.2 that the impact of the emission plume rapidly decreases relative to the turbulent background ammonia, while the emission plume itself can be detected for several kilometers as indicated by the intermittency.

4.3 Blending-distance for ammonia

Articles on ammonia measurements in close proximity of an emssion source implicitly include all relevant processes. Such studies could also provide a qualitative, perhaps more realistic, evaluation of the NH_3 blending-distance results presented here. In-field measurements show that the NH_3 molar fraction exponentially decreases with distance from the source, with measurements close to the background molar fraction after 300 to 500 m (Fowler et al., 1998; Sommer et al., 2009; Shen et al., 2016). Similar results were obtained in an intercomparison study of short-range atmospheric dispersion models by Theobald

et al. (2012), at horizontal resolutions of 25 - 50 m and receptors at 100 m intervals along four radial directions (N, E, S and W). However, such measurements are typically arranged in a few lines downwind of the source, with only a handful of measurements over a distance of 300 to 1000 m. At these short distances, plume dispersion is dominated by meandering of the plume (Nieuwstadt, 1992) and the in-plume molar fraction measurements are underestimated as a result, especially given the

395   averaging times of these measurements ranging from several hours up to multiple weeks.

Finally, we can evaluate our findings against measurement site requirements of air quality networks. The Dutch air quality network and the EMEP (European Monitoring and Evaluation Programme) network do set requirements on the minimum distance from emission sources, no references to scientific studies are provided. Back in 1990, the Dutch network required a minimum distance for NH_3 sites of 300 - 500 m from NH_3 point or area sources, depending on source strength (Boermans

400   and Erisman, 1990). This is in line with the literature on measurements in proximity of emission sources discussed earlier, but closer than the blending-distances presented here. Currently, no hard requirements are in place in the Netherlands, although the potential impact of NH_3 sources is still recognized (Wichink Kruit et al., 2021). At a European level, EMEP measurement sites require a 2 km minimum distance for measurements nearby stabling of animals and manure application, depending on the number of animals and field size (Schaug, 1988; EMEP/CCC, 2001). This 2 km distance is in line with our recommendations.

405   However, the blending-distance presented in this study indicate that distances below 2 km could also be sufficient to assure the measurement site to be regionally representative.

4.4   Towards an NH_3 virtual testbed

This study is the first which specifically addresses the regional representativity of ammonia measurements in proximity of an emission source. The systematic analysis presented in Fig. 5 and 6 can be used as a reference when interpreting in-field NH_3

410   measurements. Additionally, the simulation framework can be applied for individual locations and study the representativity of (potential new) measurement sites under the local conditions, using the concept of blending-distance. The framework presented here can be expanded to include multiple sources, each with an unique passive scalar, as well as heterogeneous surface conditions (Ouwersloot et al., 2011), to simulate the local NH_3 conditions. The DALES model has proven to be flexible, allowing for simulations of a convective, sheared convective, stable and cloud topped boundary layer (Verzijlbergh et al., 2009;

415   Heus et al., 2010).The fine scale simulation framework will be included in the Ruisdael Observatory, a nationwide observatory for measurements and modelling of the atmosphere and air quality, but can be used at any location where topography does not play an important role. The simulation framework can be a powerful tool in future ammonia research, e.g. in preparation of (emission) measurement campaigns or to improve interpretation of NH_3 (flux) measurements. Furthermore, we want to stress that the simulation framework is not limited to ammonia, but can be used for any gas for which the relevant processes

420   occur at high spatio-temporal resolution. The fine scale simulation framework will be included in the Ruisdael Observatory (https://ruisdael-observatory.nl), a Dutch nationwide observatory for measurements and modelling of the atmosphere and air quality, but can be used at any location where topography does not play an important role.

We recommend to expand the simulation framework to create a testbed to study NH_3 at high spatio-temporal resolution, including all processes relevant to the NH_3 diurnal variability. The main additions should be a dynamic parameterization

425 of the surface-atmosphere exchange, e.g. DEPAC (van Zanten et al., 2010), and a thermodynamic chemistry module, e.g. ISORROPIA version 2 (Fountoukis and Nenes, 2007). With these additions, on top of the existing possibility to distinguish between background and emitted NH_3, the fine scale simulation framework with explicitly resolved turbulence will be well suited to study short-range dispersion of ammonia, e.g. deposition in close proximity to emission sources. Such studies are typically performed using models where turbulence is parameterized or using Gaussian plume models (Loubet et al., 2006;

430 Sommer et al., 2009; van der Swaluw et al., 2017). Furthermore, the addition of a thermodynamic chemistry module can lead to new insights on NH_3 flux measurements. The equilibrium molar fractions of the NH_3 gas-aerosol transformations depend on the atmospheric temperature and humidity, resulting in a near-surface molar fraction gradient. This gradient leads to an underestimation of the NH_3 deposition flux of about 0.02 μg m^{-2}s^{-1} when using the flux-gradient method (Nemitz et al., 2004). With these additions to the simulation framework, the virutal NH_3 testbed can be used improve the interpretation of NH_3 flux

435 measurements.

5 Conclusions

This paper presents a fine scale simulation framework with which we assess the regional representativity of NH_3 molar fraction and flux measurements in proximity of a typical NH_3 emission source. We aim to translate concepts from the fields of plume dispersion and fine scale simulations to a practical application in the field of NH_3 measurements, including realistic represen-

440 tations of NH_3 surface-atmosphere exchange and chemical gas-aerosol transformations. The concept of a blending-distance is introduced to systematically analyze the impact of the emitted NH_3 on simulated measurements, relative to a background concentration. Following this approach, we define a first-order estimate of a minimum distance requirement between regional representative measurements and a typical NH_3 emission source.

By means of fine scale simulation of atmospheric NH_3, we investigate the representativity of NH_3 measurements from

445 kilometer to meter scales in proximity of a typical emission source. The fine scale simulation framework presented has proven to be a powerful and flexible tool for future research on ammonia, or any gas for which the relevant processes occur at high spatio-temporal resolution. The simulation framework with explicitly resolved turbulence not only enables us to quantify the variability in NH_3 measurements, but also to analyze and quantify the individual contribution of the emitted NH_3. The concept of blending-distance presents a consistent criterium, based on second order statistics, for the minimum distance at which the

450 impact of the emitted NH_3 is estimated to be indistinguishable from the variability of the background NH_3. A systematic analysis of the blending-distance shows a strong sensitivity to the emission strenght, deposition and the threshold level used in the calculation, and to the stability of the (convective or shear dominated) boundary layer. Furthermore, we find that the blending-distances differ for NH_3 molar fraction and flux measurements, with flux measurements being more sensitive to the NH_3 emission plume. Following this sensitivity analysis, we conclude that NH_3 measurements should be taken at a minimum

455 distance of 0.5 - 2.5 km or 1 - 3.5 km distance from an emission source, for measurements of the NH_3 molar fraction or flux respectively.

Code availability. Model code and processing scripts will be made availabile upon publication.

Author contributions. RS and JV worked on the conceptualization and developed the methodology of the numerical experiments. RS made adaptations to the software used in this study and performed the numerical experiments, and analyzed and visualized of the data. The manuscript draft is written by RS and reviewed by both JV and MZ. Finally, the project was supervized by JV and MZ.

Competing interests. The authors declare that they have no conflict of interest.

Acknowledgements. We thank Bart van Stratum (WUR) for his assistance with setting-up the DALES model and for his support with the modifications of the model. This research was financed by the Dutch National Institute of Public Health and the Environment (RIVM) within the framework of the Project 36.7: Monitoring of dry ammonia deposition, which is performed by order, and for the account, of the Dutch Ministry of Agriculture, Nature and Food Quality. The numerical simulations were performed with the supercomputer facilities at SURFsara and financially sponsored by the Netherlands Organisation for Scientific Research (NWO) Physical Science Division (project number 2021/ENW/01081379).

References

aan de Brugh, J. M. J., Henzing, J. S., Schaap, M., Morgan, W. T., van Heerwaarden, C. C., Weijers, E. P., Coe, H., and Krol, M. C.:

470   Modelling the partitioning of ammonium nitrate in the convective boundary layer, Atmospheric Chemistry and Physics, 12, 3005–3023, https://doi.org/10.5194/acp-12-3005-2012, 2012.

aan de Brugh, J. M. J., Ouwersloot, H. G., Vilà-Guerau de Arellano, J., and Krol, M. C.: A large-eddy simulation of the phase transition of ammonium nitrate in a convective boundary layer, Journal of Geophysical Research: Atmospheres, 118, 826–836, https://doi.org/10.1002/jgrd.50161, 2013.

475 Anys, M., Ullrich, B., Gager, M., and Pinterits, M.: European Union emission inventory report 1990-2018: under the UNECE Convention on Long-range Transboundary Air Pollution, Tech. Rep. TH-AL-20-013-EN-N, European Environment Agency, Kongens Nytorv 6, 1050 Copenhagen K, Denmark, https://www.eea.europa.eu/ds_resolveuid/c48fe5a189e5484095dcb509da927a36, 2020.

Ardeshiri, H., Cassiani, M., Park, S. Y., Stohl, A., Pisso, I., and Dinger, A. S.: On the Convergence and Capability of the Large-Eddy Simulation of Concentration Fluctuations in Passive Plumes for a Neutral Boundary Layer at Infinite Reynolds Number, Boundary-Layer

480   Meteorology, 176, 291 – 327, https://doi.org/10.1007/s10546-020-00537-6, 2021.

Barad, M. L.: Project Prairie Grass, a field program in diffusion. Volume 1, Tech. Rep. No. 59, Vol I , Report AFCRC-TR-58-235(I), AIR FORCE CAMBRIDGE RESEARCH LABS, https://www.harmo.org/jsirwin/PGrassVolumeI.pdf, 1958.

Barbaro, E., Vilà-Guerau de Arellano, J., Ouwersloot, H. G., Schröter, J. S., Donovan, D. P., and Krol, M. C.: Aerosols in the convective boundary layer: Shortwave radiation effects on the coupled land-atmosphere system, Journal of Geophysical Research: Atmospheres, 119,

485 5845–5863, https://doi.org/10.1002/2013JD021237, 2014.

Barbaro, E., Krol, M., and Vilà-Guerau de Arellano, J.: Numerical simulation of the interaction between ammonium nitrate aerosol and convective boundary-layer dynamics, Atmospheric Environment, 105, 202–211, https://doi.org/10.1016/j.atmosenv.2015.01.048, 2015.

Behera, S. N., Sharma, M., Aneja, V. P., and Balasubramanian, R.: Ammonia in the atmosphere: a review on emission sources, atmospheric chemistry and deposition on terrestrial bodies, Environmental Science and Pollution Researc, 20, 8092 – 8131,

490   https://doi.org/10.1007/s11356-013-2051-9, 2013.

Berkhout, A. J. C., Swart, D. P. J., Volten, H., Gast, L. F. L., Haaima, M., Verboom, H., Stefess, G., Hafkenscheid, T., and Hoogerbrugge, R.: Replacing the AMOR with the miniDOAS in the ammonia monitoring network in the Netherlands, Atmospheric Measurement Techniques, 10, 4099–4120, https://doi.org/10.5194/amt-10-4099-2017, 2017.

Boermans, G. M. F. and Erisman, J. W.: Meetstrategieontwikkeling voor het representativiteitsonderzoek als onderdeel van het additioneel

495 meetprogramma ammoniak: fenomenologie van NH3 en meetritsimulaties, Tech. Rep. 222105001, National Institute for Public Health and the Environment (RIVM), Antonie van Leeuwenhoeklaan 9, 3721, MA Bilthoven, the Netherlands, http://hdl.handle.net/10029/255566, 1990.

Cassiani, M., Bertagni, M., Marro, M., and Salizzoni, P.: Concentration Fluctuations from Localized Atmospheric Releases, Boundary-Layer Meteorology, 177, 461–510, https://doi.org/10.1007/s10546-020-00547-4, 2020.

500 Dosio, A. and Vilà-Guerau de Arellano, J.: Statistics of Absolute and Relative Dispersion in the Atmospheric Convective Boundary Layer: A Large-Eddy Simulation Study, Journal of the Atmospheric Sciences, 63, 1253 – 1272, https://doi.org/10.1175/JAS3689.1, 2006.

Dosio, A., Vilà-Guerau de Arellano, J., Holtslag, A. A. M., and Builtjes, P. J. H.: Dispersion of a Passive Tracer in Buoyancy- and Shear-Driven Boundary Layers, Journal of Applied Meteorology, 42, 1116 – 1130, https://doi.org/10.1175/1520-0450(2003)042<1116:DOAPTI>2.0.CO;2, 2003.

505   EMEP/CCC: EMEP manual for sampling and chemical analysis, Tech. Rep. EMEP/CCC-Report 1/95, O-7726, Chemical Co-ordination Centre of EMEP (EMEP/CCC), https://projects.nilu.no/ccc/manual/download/cccr1-95rev.pdf, 2001.

Erisman, J. and Schaap, M.: The need for ammonia abatement with respect to secondary PM reductions in Europe, Environmental Pollution, 129, 159–163, https://doi.org/10.1016/j.envpol.2003.08.042, 2004.

Erisman, J. W., Galloway, J. N., Seitzinger, S., Bleeker, A., Dise, N. B., Petrescu, A. M. R., Leach, A. M., and de Vries, W.: Consequences of
510   human modification of the global nitrogen cycle, Philosophical Transactions of the Royal Society B: Biological Sciences, 368, 20130 116, https://doi.org/10.1098/rstb.2013.0116, 2013.

Fountoukis, C. and Nenes, A.: ISORROPIA II: a computationally efficient thermodynamic equilibrium model for K^+-Ca^{2+}-Mg^{2+}-NH_4^+-Na^+-SO_4^{2-}-NO_3^--Cl^--H_2O aerosols, Atmos. Chem. Phys., 7, 4639–4659, https://doi.org/10.5194/acp-7-4639-2007, 2007.

Fowler, D., Pitcairn, C. E. R., Sutton, M. A., Flechard, C., Loubet, B., Coyle, M., and Munro, R. C.: The mass budget of atmospheric ammonia
515   in woodland within 1 km of livestock buildings, Environmental Pollution, 102, 343 – 348, https://doi.org/10.1016/S0269-7491(98)80053-5, 1998.

Gailis, R. M., Hill, A., Yee, E., and Hilderman, T.: Extension of a fluctuating plume model of tracer dispersion to a sheared boundary layer and to a large array of obstacles, Boundary-Layer Meteorology, 122, 577–607, https://doi.org/10.1007/s10546-006-9118-9, 2007.

Heus, T., van Heerwaarden, C. C., Jonker, H. J. J., Pier Siebesma, A., Axelsen, S., van den Dries, K., Geoffroy, O., Moene, A. F., Pino, D.,
520   de Roode, S. R., and Vilà-Guerau de Arellano, J.: Formulation of the Dutch Atmospheric Large-Eddy Simulation (DALES) and overview of its applications, Geoscientific Model Development, 3, 415–444, https://doi.org/10.5194/gmd-3-415-2010, 2010.

Kljun, N., Kormann, R., Rotach, M. W., and Meixer, F. X.: Comparison of the lagrangian footprint model LPDM-B with an analytical footprint model, Boundary-Layer Meteorology, 106, 349–355, https://doi.org/10.1023/A:1021141223386, 2003.

Kulmala, M., Asmi, A., Lappalainen, H. K., Baltensperger, U., Brenguier, J.-L., Facchini, M. C., Hansson, H.-C., Hov, Ø., O'Dowd, C. D.,
525   Pöschl, U., Wiedensohler, A., Boers, R., Boucher, O., de Leeuw, G., Denier van der Gon, H. A. C., Feichter, J., Krejci, R., Laj, P., Lihavainen, H., Lohmann, U., McFiggans, G., Mentel, T., Pilinis, C., Riipinen, I., Schulz, M., Stohl, A., Swietlicki, E., Vignati, E., Alves, C., Amann, M., Ammann, M., Arabas, S., Artaxo, P., Baars, H., Beddows, D. C. S., Bergström, R., Beukes, J. P., Bilde, M., Burkhart, J. F., Canonaco, F., Clegg, S. L., Coe, H., Crumeyrolle, S., D'Anna, B., Decesari, S., Gilardoni, S., Fischer, M., Fjaeraa, A. M., Fountoukis, C., George, C., Gomes, L., Halloran, P., Hamburger, T., Harrison, R. M., Herrmann, H., Hoffmann, T., Hoose, C., Hu, M., Hyvärinen, A.,
530   Hõrrak, U., Iinuma, Y., Iversen, T., Josipovic, M., Kanakidou, M., Kiendler-Scharr, A., Kirkevåg, A., Kiss, G., Klimont, Z., Kolmonen, P., Komppula, M., Kristjánsson, J.-E., Laakso, L., Laaksonen, A., Labonnote, L., Lanz, V. A., Lehtinen, K. E. J., Rizzo, L. V., Makkonen, R., Manninen, H. E., McMeeking, G., Merikanto, J., Minikin, A., Mirme, S., Morgan, W. T., Nemitz, E., O'Donnell, D., Panwar, T. S., Pawlowska, H., Petzold, A., Pienaar, J. J., Pio, C., Plass-Duelmer, C., Prévôt, A. S. H., Pryor, S., Reddington, C. L., Roberts, G., Rosenfeld, D., Schwarz, J., Seland, Ø., Sellegri, K., Shen, X. J., Shiraiwa, M., Siebert, H., Sierau, B., Simpson, D., Sun, J. Y., Topping, D., Tunved,
535   P., Vaattovaara, P., Vakkari, V., Veefkind, J. P., Visschedijk, A., Vuollekoski, H., Vuolo, R., Wehner, B., Wildt, J., Woodward, S., Worsnop, D. R., van Zadelhoff, G.-J., Zardini, A. A., Zhang, K., van Zyl, P. G., Kerminen, V.-M., S Carslaw, K., and Pandis, S. N.: General overview: European Integrated project on Aerosol Cloud Climate and Air Quality interactions (EUCAARI) - integrating aerosol research from nano to global scales, Atmospheric Chemistry and Physics, 11, 13 061–13 143, https://doi.org/10.5194/acp-11-13061-2011, 2011.

Loubet, B., Cellier, P., Milford, C., and Sutton, M. A.: A coupled dispersion and exchange model for short-range dry deposition of atmo-
540   spheric ammonia, Quarterly Journal of the Royal Meteorological Society, 132, 1733–1763, https://doi.org/10.1256/qj.05.73, 2006.

Mensah, A. A., Holzinger, R., Otjes, R., Trimborn, A., Mentel, T. F., ten Brink, H., Henzing, B., and Kiendler-Scharr, A.: Aerosol chemical composition at Cabauw, The Netherlands as observed in two intensive periods in May 2008 and March 2009, Atmospheric Chemistry and Physics, 12, 4723–4742, https://doi.org/10.5194/acp-12-4723-2012, 2012.

Mylne, K. R. and Mason, P. J.: Concentration fluctuation measurements in a dispersing plume at a range of up to 1000 m, Quarterly Journal of the Royal Meteorological Society, 117, 177–206, https://doi.org/10.1002/qj.49711749709, 1991.

Nemitz, E., Sutton, M. A., Wyers, G. P., Otjes, R. P., Mennen, M. G., van Putten, E. M., and Gallagher, M. W.: Gas-particle interactions above a Dutch heathland: II. Concentrations and surface exchange fluxes of atmospheric particles, Atmospheric Chemistry and Physics, 4, 1007–1024, https://doi.org/10.5194/acp-4-1007-2004, 2004.

Nieuwstadt, F.: A large-eddy simulation of a line source in a convective atmospheric boundary layer—I. Dispersion characteristics, Atmospheric Environment. Part A. General Topics, 26, 485–495, https://doi.org/10.1016/0960-1686(92)90331-E, 1992.

Ouwersloot, H. G., Vilà-Guerau de Arellano, J., van Heerwaarden, C. C., Ganzeveld, L. N., Krol, M. C., and Lelieveld, J.: On the segregation of chemical species in a clear boundary layer over heterogeneous land surfaces, Atmospheric Chemistry and Physics, 11, 10 681–10 704, https://doi.org/10.5194/acp-11-10681-2011, 2011.

Ouwersloot, H. G., Moene, A. F., Attema, J. J., and Vilà-Guerau de Arellano, J.: Large-Eddy Simulation Comparison of Neutral Flow Over a Canopy: Sensitivities to Physical and Numerical Conditions, and Similarity to Other Representations, Boundary-Layer Meteorology, 162, 71–89, https://doi.org/10.1007/s10546-016-0182-5, 2017.

Rannik, ., Aubinet, M., Kurbanmuradov, O., Sabelfeld, K. K., Markkanen, T., and Vesala, T.: Footprint Analysis For Measurements Over A Heterogeneous Forest, Boundary-Layer Meteorology, 97, 137–166, https://doi.org/10.1023/A:1002702810929, 2000.

Ražnjević, A., van Heerwaarden, C., van Stratum, B., Hensen, A., Velzeboer, I., van den Bulk, P., and Krol, M.: Technical note: Interpretation of field observations of point-source methane plume using observation-driven large-eddy simulations, Atmospheric Chemistry and Physics Discussions, 2021, 1–29, https://doi.org/10.5194/acp-2021-614, 2021.

Remmelink, G., van Middelkoop, J., Ouweltjes, W., and Wemmenhove, H.: Handboek melkveehouderij 2020/21, no. 44 in Handboek / Wageningen Livestock Research, Wageningen Livestock Research, https://doi.org/10.18174/529557, over the year 2019/20, 2020.

RIVM: Landbouw, Emissiefactoren diercategorieën, Hoofdcategorie A: Rundvee, https://www.infomil.nl/onderwerpen/landbouw/emissiearme-stalsystemen/emissiefactoren-per/map-staltypen/hoofdcategorie/, accessed: 2021-01-28, 2021.

Sauter, F., van Zanten, M., van der Swaluw, E., Aben, J., de Leeuw, F., and van Jaarsveld, H.: The OPS-model: Description of OPS 4.5.2, Tech. rep., National Institute for Public Health and the Environment (RIVM, https://www.rivm.nl/media/ops/OPS-model.pdf, 2018.

Schaap, M., Timmermans, R. M. A., Roemer, M., Boersen, G. A. C., Builtjes, P. J. H., Sauter, F. J., Velders, G. J. M., and Beck, J. P.: The LOTOS–EUROS model: description, validation and latest developments, International Journal of Environment and Pollution, 32, 270–290, https://doi.org/10.1504/IJEP.2008.017106, 2008.

Schaug, J.: Quality assurance plane for EMEP, Tech. Rep. EMEP/CCC-Report 1/88, Norwegian Institute for Air Research, https://projects.nilu.no/ccc/reports/cccr1-88.pdf, 1988.

Schulte, R., van Zanten, M., Rutledge-Jonker, S., Swart, D., Wichink Kruit, R., Krol, M., van Pul, W., and Vilà-Guerau de Arellano, J.: Unraveling the diurnal atmospheric ammonia budget of a prototypical convective boundary layer, Atmospheric Environment, 249, 118 153, https://doi.org/10.1016/j.atmosenv.2020.118153, 2021.

Shah, A., Pitt, J. R., Ricketts, H., Leen, J. B., Williams, P. I., Kabbabe, K., Gallagher, M. W., and Allen, G.: Testing the near-field Gaussian plume inversion flux quantification technique using unmanned aerial vehicle sampling, Atmospheric Measurement Techniques, 13, 1467–1484, https://doi.org/10.5194/amt-13-1467-2020, 2020.

Shen, J., Chen, D., Bai, M., Sun, J., Coates, T., Lam, S. K., and Li, Y.: Ammonia deposition in the neighbourhood of an intensive cattle feedlot in Victoria, Australia, Sci Rep, 6, 2045–2322, https://doi.org/10.1038/srep32793, 2016.

Simpson, D., Benedictow, A., Berge, H., Bergström, R., Emberson, L. D., Fagerli, H., Flechard, C. R., Hayman, G. D., Gauss, M., Jonson, J. E., Jenkin, M. E., Nýiri, A., Richter, C., Semeena, V. S., Tsyro, S., Tuovinen, J.-P., Valdebenito, ., and Wind, P.: The EMEP MSC-W chemical transport model - technical description, Atmospheric Chemistry and Physics, 12, 7825 – 7865, https://doi.org/10.5194/acp-12-7825-2012, 2012.

Smit, L. A. M. and Heederik, D.: Impacts of Intensive Livestock Production on Human Health in Densely Populated Regions, GeoHealth, 1, 272–277, https://doi.org/10.1002/2017GH000103, 2017.

Sommer, S., Østergård, H., Løfstrøm, P., Andersen, H., and Jensen, L.: Validation of model calculation of ammonia deposition in the neighbourhood of a poultry farm using measured NH3 concentrations and N deposition, Atmospheric Environment, 43, 915–920, https://doi.org/10.1016/j.atmosenv.2008.10.045, 2009.

Stokstad, E.: Nitrogen crisis threatens Dutch environment- and economy, Science, 366, 1180–1181, https://doi.org/10.1126/science.366.6470.1180, 2019.

Stolk, A., Noordijk, H., and van Zanten, M.: Drogedepositiemetingen van ammoniak in Natura 2000-gebied Bargerveen, Tech. Rep. 680029001, National Institute for Public Health and the Environment (RIVM), Antonie van Leeuwenhoeklaan 9, 3721, MA Bilthoven, the Netherlands, https://rivm.openrepository.com/handle/10029/320523, 2014.

Sutton, M. A., Erisman, J. W., Dentener, F., and Möller, D.: Ammonia in the environment: From ancient times to the present, Environmental Pollution, 156, 583 – 604, https://doi.org/10.1016/j.envpol.2008.03.013, 2008.

Theobald, M. R., Løfstrøm, P., Walker, J., Andersen, H. V., Pedersen, P., Vallejo, A., and Sutton, M. A.: An intercomparison of models used to simulate the short-range atmospheric dispersion of agricultural ammonia emissions, Environmental Modelling & Software, 37, 90–102, https://doi.org/10.1016/j.envsoft.2012.03.005, 2012.

van Bruggen, C., Bannink, A., Groenestein, C., Huijsmans, J., Lagerwerf, L., Luesink, H., Ros, M., Velthof, G., Vonk, J., and van der Zee, T.: Emissies naar lucht uit de landbouw berekend met NEMA voor 1990-2019, no. 203 in WOt-technical report, Wettelijke Onderzoekstaken Natuur & Milieu, https://doi.org/10.18174/544296, project number WOT-04-008-031.01 and WOT-04-008-025.02, 2021.

van der Peet, G., Leenstra, F., Vermeij, I., Bondt, N., Puister, L., and van Os, J.: Feiten en cijfers over de Nederlandse veehouderijsectoren 2018, no. 1134 in Wageningen Livestock Research rapport, Wageningen Livestock Research, https://doi.org/10.18174/464128, 2018.

van der Swaluw, E., de Vries, W., Sauter, F., Aben, J., Velders, G., and van Pul, A.: High-resolution modelling of air pollution and deposition over the Netherlands with plume, grid and hybrid modelling, Atmospheric Environment, 155, 140–153, https://doi.org/10.1016/j.atmosenv.2017.02.009, 2017.

van Jaarsveld, J.: The Operational Priority Substances model: Description and validation of OPS-Pro 4.1, Tech. Rep. 500045001, National Institute for Public Health and the Environment (RIVM), Antonie van Leeuwenhoeklaan 9, 3721, MA Bilthoven, the Netherlands, https://www.rivm.nl/publicaties/operational-priority-substances-model, 2004.

Van Oss, R., Duyzer, J., and Wyers, P.: The influence of gas-to-particle conversion on measurements of ammonia exchange over forest, Atmospheric Environment, 32, 465–471, https://doi.org/10.1016/S1352-2310(97)00280-X, 1998.

van Zanten, M., Wichink Kruit, R., Hoogerbrugge, R., Van der Swaluw, E., and van Pul, W.: Trends in ammonia measurements in the Netherlands over the period 1993–2014, Atmospheric Environment, 148, 352–360, https://doi.org/10.1016/j.atmosenv.2016.11.007, 2017.

615 van Zanten, M. C., Sauter, F. J., Wichink Kruit, R. J., van Jaarsveld, J. A., and van Pul, W. A. J.: Description of the DEPAC module: Dry deposition modelling with DEPAC-GCN2010, Tech. Rep. 680180001, National Institute for Public Health and the Environment (RIVM), https://www.rivm.nl/bibliotheek/rapporten/680180001.pdf, 2010.

Verzijlbergh, R. A., Jonker, H. J. J., Heus, T., and Vilà-Guerau de Arellano, J.: Turbulent dispersion in cloud-topped boundary layers, Atmospheric Chemistry and Physics, 9, 1289–1302, https://doi.org/10.5194/acp-9-1289-2009, 2009.

620 Vesala, T., Kljun, N., Rannik, ., Rinne, J., Sogachev, A., Markkanen, T., Sabelfeld, K., Foken, T., and Leclerc, M.: Flux and concentration footprint modelling: State of the art, Environmental Pollution, 152, 653–666, https://doi.org/10.1016/j.envpol.2007.06.070, 2008.

Vonk, J., Arets, E., Bannink, A., van Bruggen, C., Groenestein, C., Huijsmans, J., Lagerwerf, L., Luesink, H., Ros, M., Schelhaas, M., van der Zee, T., and Velthof, G.: Referentieraming van emissies naar de lucht uit landbouw en landgebruik tot 2030, met doorkijk naar 2035: Achtergronddocument bij de Klimaat- en Energieverkenning 2020, no. 1278 in Rapport / Wageningen Livestock Research, Wageningen
625 Livestock Research, https://doi.org/10.18174/533503, 2020.

Vrieling, A. and Nieuwstadt, F.: Turbulent dispersion from nearby point sources—interference of the concentration statistics, Atmospheric Environment, 37, 4493–4506, https://doi.org/10.1016/S1352-2310(03)00576-4, 2003.

Wichink Kruit, R. and van Pul, W. A. J.: Ontwikkelingen in de stikstofdepositie, https://doi.org/10.21945/RIVM-2018-0117, 2018.

Wichink Kruit, R., Bleeker, A., Braam, M., van Goethem, T., Hoogerbrugge, R., Rutledge-Jonker, S., Stefess, G., Stolk, A., van der Swaluw,
630 E., Voogt, M., and van Pul, A.: Op weg naar een optimale meetstrategie voor stikstof, https://doi.org/10.21945/RIVM-2021-0118, 2021.

Wichink Kruit, R. J., van Pul, W. A. J., Otjes, R. P., Hofschreuder, P., Jacobs, A. F. G., and Holtslag, A. A. M.: Ammonia fluxes and derived canopy compensation points over non-fertilized agricultural grassland in The Netherlands using the new GRadient Ammonia - High Accuracy - Monitoring (GRAHAM), Atmospheric Environment, 41, 1275 – 1287, https://doi.org/10.1016/j.atmosenv.2006.09.039, 2007.

Wichink Kruit, R. J., van Pul, W. A. J., Sauter, F. J., van den Broek, M., E., N., Sutton, M. A., Krol, M., and Holtslag, A. A. M.: Modeling the
635 surface–atmosphere exchange of ammonia, Atmospheric Environment, 44, 945 – 957, https://doi.org/10.1016/j.atmosenv.2009.11.049, 2010.

WUR: Dutch Farm Accountancy Data Network, agriculture, https://www.agrimatie.nl/Binternet.aspx?ID=2&Bedrijfstype=2%403& SelectedJaren=2020&GroteKlassen=Alle+bedrijven, accessed: 2021-06-21, 2021.